

Article

A Hybrid Convolutional and Recurrent Neural Network for Multi-Sensor Pile Damage Detection with Time Series

Juntao Wu ¹, M. Hesham El Naggar ² and Kuihua Wang ^{1,*}¹ College of Civil Engineering and Architecture, Zhejiang University, Hangzhou 310058, China² Geotechnical Research Centre, University of Western Ontario, London, ON N6A 5B9, Canada

* Correspondence: zdwkh0618@zju.edu.cn

Abstract: Machine learning (ML) algorithms are increasingly applied to structure health monitoring (SHM) problems. However, their application to pile damage detection (PDD) is hindered by the complexity of the problem. A novel multi-sensor pile damage detection (MSPDD) method is proposed in this paper to extend the application of ML algorithms in the automatic identification of PDD. The time-series signals collected by multiple sensors during the pile integrity test are first processed by the traveling wave decomposition (TWD) theory and are then input into a hybrid one-dimensional (1D) convolutional and recurrent neural network. The hybrid neural network can achieve the automatic multi-task identification of pile damage detection based on the time series of MSPDD results. Finally, the analytical solution-based sample set is utilized to evaluate the performance of the proposed hybrid model. The outputs of the multi-task learning framework can provide a detailed description of the actual pile quality and provide strong support for the classification of pile quality as well.

Keywords: pile damage detection; multiple sensors; convolutional neural network; recurrent neural network; analytical solution



Citation: Wu, J.; El Naggar, M.H.; Wang, K. A Hybrid Convolutional and Recurrent Neural Network for Multi-Sensor Pile Damage Detection with Time Series. *Sensors* **2024**, *24*, 1190. <https://doi.org/10.3390/s24041190>

Academic Editor: Gilbert-Rainer Gillich

Received: 23 January 2024

Revised: 31 January 2024

Accepted: 9 February 2024

Published: 11 February 2024



Copyright: © 2024 by the authors. Licensee MDPI, Basel, Switzerland. This article is an open access article distributed under the terms and conditions of the Creative Commons Attribution (CC BY) license (<https://creativecommons.org/licenses/by/4.0/>).

1. Introduction

Pile foundations play an important role in onshore and offshore engineering projects. Therefore, it is necessary to evaluate the integrity and quality of pile foundations and thus ensure the safety of supported superstructures. To detect the integrity of reinforced concrete (RC) piles, a variety of non-destructive testing techniques have been proposed successively, such as the low-strain pile integrity test (PIT) [1–4], sonic cross-hole logging (SCL) [5–8] and the parallel seismic (PS) method [9–14]. The existence of potential pile defects and unknown pile lengths can be detected by one method or a combination of multiple methods. Meanwhile, these techniques still have certain limitations, e.g., the PIT and lateral PIT [15,16] methods are convenient to implement, however the results may not be as reliable in the case of shallow and multiple defects, where the pile toe reflection is inevitably affected by the defect above. Similarly, the SCL test can be conducted along the entire length of the pile, but it only examines the area between the sonic logging tubes and cannot reflect the actual mechanical information of the pile cross-section. The PS results incorporate the whole mechanical information of both the pile and the surrounding soil, but the test requires significant preparatory work, which increases the cost. At the same time, most of these methods rely heavily on the operators' experience, which is not conducive to automatic identification.

Machine learning (ML) algorithms are increasingly applied to structure health monitoring (SHM) [17–20]. Several researchers employed ML algorithms, such as support vector machine (SVM) and artificial neural network (ANN), to automatically recognize damage to steel truss [21,22], steel frames [23,24] and bridge structures [25–27]. Given the acceleration and velocity responses that are collected from the structure are time-series signals, there are two major ways to extract vibration-based features. The first method extracts

statistical features from time-series signals and uses them as the input to ML algorithm frameworks [28–30]. The second method utilizes the one-dimensional (1D) convolutional neural network (CNN) to automatically extract the features [31–34]. The 1DCNN has the same advantages as the CNN and is capable of learning more comprehensive features (i.e., less susceptible to subjective experience). However, compared with superstructure monitoring, there are scarce studies on the application of ML algorithms to pile damage detection (PDD) due to the challenges of pile quality detection. Generally, existing pile detection techniques and their test results are not suitable for data-driven analysis (e.g., the test excitations of the PIT and PS methods are applied manually and are not repeatable; the reliability of one-sensor tests (PIT and lateral PIT) at the pile top is susceptible, and the PS test results with multiple sensors at desired depths are influenced by the structure above the sensors).

To overcome the limitations of existing pile detection techniques and further extend the application of ML algorithms in the automatic identification of PDD, a novel multi-sensor pile damage detection (MSPDD) method is proposed in this paper to evaluate the integrity of onshore and offshore pile foundations. Combined with the traveling wave decomposition (TWD) theory, the normalized MSPDD results can eliminate the vibration of the structure above the sensors. In order to handle the time-series MSPDD results, a hybrid one-dimensional (1D) convolutional and recurrent neural network is developed herein to automatically conduct multi-task pile damage detection. Finally, the analytical solution-based sample set is utilized to evaluate the performance of the proposed hybrid neural network.

2. Multi-Sensor Pile Damage Detection (MSPDD) Method

In order to overcome the limitations of existing pile quality detection methods and further integrate them with machine learning (ML) algorithms, a novel multi-sensor pile damage detection (MSPDD) method is proposed herein to evaluate the integrity of onshore and offshore pile foundations.

2.1. Operation Steps

In the MSPDD method, multiple (more than three) equally spaced sensors are installed along the pile shaft in the depth range of interest and are used to simultaneously receive the dynamic velocity responses induced by the test hammer strike. Different from the traditional pile integrity test (PIT) that utilizes only one sensor located at/near the pile top, employing multiple sensors at various depths gathers more information and is more flexible and reliable for complicated testing conditions. Combined with the traveling wave decomposition (TWD) theory [35,36] developed for equally spaced sensors, the MSPDD results can eliminate the effect of vibration of the structure above the sensors and thus reveal the integrity of the remainder below. Consequently, the MSPDD method and its test results are almost unaffected by shallow defects, enlarged pile tops and superstructures. Therefore, it can be utilized to evaluate piles with multiple defects and extremely long lengths.

To achieve the installation of multiple sensors at desired depths and make use of existing test techniques, some implementation ideas are proposed for onshore and offshore piles [37–39]. For example, as depicted in Figure 1a, if a reinforced concrete (RC) pile is qualified for the cross-hole sonic logging (CSL) test, a series of hydrophones (commonly used in the PS method) can be plugged into one of the water-filled sonic logging tubes located below the known defect (e.g., an enlarged pile top or a detected defect); Figure 1b demonstrates a series of transducers installed along the outer surface of an offshore pile to conduct the MSPDD test, where the sensors below the superstructure can remove the effects of the above structure after signal post-processing (as will be introduced in the ensuing section). For an RC pipe pile, the sensors can be installed on the pile's inner wall. Even though the installation methods of sensors may be different considering various pile types and service environments, the multiple sensors are generally arranged at a specific depth

with equal spacing to receive signals simultaneously. In addition, the receiving direction of the sensors should be consistent with the major direction of the hammer strike.

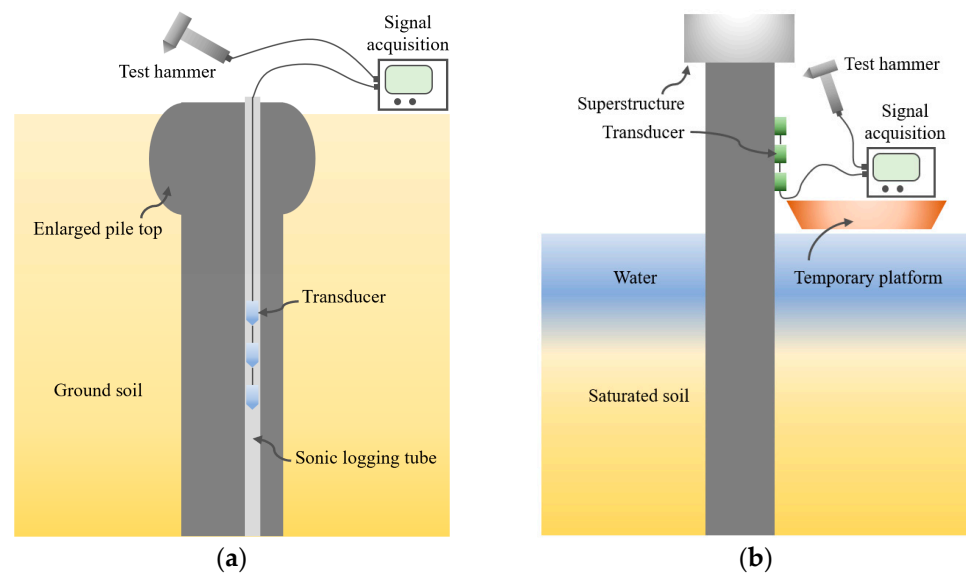


Figure 1. Layout of multiple sensors installed on (a) a pile with available sonic logging tubes; and (b) an extended pile shaft with superstructure.

2.2. Signal Post-Processing

After collecting a series of signals with a multi-channel data acquisition system (as demonstrated in Figure 2a), the traveling wave decomposition (TWD) theory is utilized to implement the post-processing. Considering three neighboring sensors as an example, the time-series signal can be expressed as the sum of downward- and upward-traveling waves, i.e.,

$$v(z, t) = \zeta(z - C_p t) + \eta(z + C_p t) \quad (1)$$

where z is the depth variable whose positive direction is downward; t is the time variable; $\zeta(\cdot)$ and $\eta(\cdot)$ are the downward- and upward-traveling waveforms and C_p denotes the one-dimensional traveling wave velocity of the RC pile (i.e., elastic wave velocity or shear wave propagating velocity corresponding to sensors collecting vertical or lateral components).

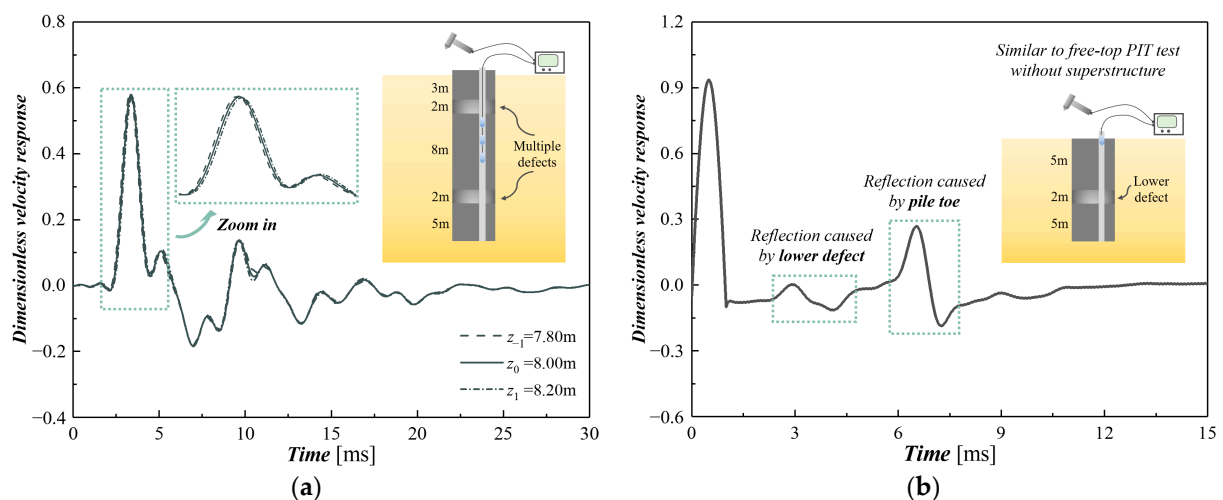


Figure 2. Post-processing for MSPDD method: (a) raw data collected by multiple sensors; (b) reconstructed MSPDD result employing traveling wave decomposition (TWD) theory.

Since the effect of pile damping on the velocity amplitude of propagating waves is negligible due to the relatively small spacing between adjacent sensors (no more than 0.50 m in practice), the time-series signal collected by neighboring sensors satisfies the following relation:

$$v(m, n) = \zeta(m, n) + \eta(m, n) = \zeta(z_0 + m\Delta z, t + n\Delta t) + \eta(z_0 + m\Delta z, t + n\Delta t) \quad (2)$$

where $m = -1, 0, 1$; z_0 denotes the depth of the middle sensor; Δz is the spacing between adjacent sensors; $\Delta t = \Delta z/C_p$; n is a non-negative integer because of the causality of the linear time-invariant (LTI) system.

The traveling downward and upward waves yield the following:

$$\begin{cases} \zeta(m, n) = \zeta(m-1, n-1) \\ \eta(m, n) = \eta(m+1, n-1) \end{cases}, n \geq 1 \quad (3)$$

Comparing the velocities of the lower ($z = z_0 + \Delta z$) and upper ($z = z_0 - \Delta z$) sensors at $t = t + \Delta t$ with the velocity of the middle sensor ($z = z_0$), respectively, we have

$$\begin{cases} v(1, 1) - v(0, 0) = \eta(1, 1) - \eta(0, 0) = \eta(0, 2) - \eta(0, 0) \\ v(-1, 1) - v(0, 0) = \zeta(-1, 1) - \zeta(0, 0) = \zeta(0, 2) - \zeta(0, 0) \end{cases} \quad (4)$$

Since $v(0, 0)$, $v(1, 1)$ and $v(-1, 1)$ are known data collected by multiple sensors, the downward and upward waves passing through the middle sensor (i.e., $\zeta(0, 0)$ and $\eta(0, 0)$) can be solved by iterative calculation. By regarding the downward and upward waves as the input and output, the pseudo-frequency response (PFR) function for the structure below the sensors can be expressed as follows:

$$H_v = \frac{\bar{\eta}(0, 0)}{\bar{\zeta}(0, 0)} + 1 \quad (5)$$

where $\bar{\zeta}(0, 0)$ and $\bar{\eta}(0, 0)$ are the Fourier transform (FT) of $\zeta(0, 0)$ and $\eta(0, 0)$, respectively; the addition of unity is employed herein to reproduce the downward (incident) wave, which makes the PFR function closer to the conventional frequency response (FR) function.

The PFR function contains almost all the mechanics information below the sensors while eliminating the effect of the upper structure. A normalized semi-sine fictitious excitation with a unit amplitude and user-defined duration is then utilized to reconstruct the MSPDD result (as depicted in Figure 2b). This is the same as the result derived from a free-top PIT or lateral PIT [15,16] applied to a pile foundation that has no superstructure.

3. Multi-Task Learning Framework for Time-Series MSPDD Results

Benefiting from the TWD theory and the PFR function, the time-series MSPDD results, which are free from disturbances caused by environment, temperature and equipment, can reveal the reflections caused by the pile toe or pile defect below the sensors. Moreover, in post-processing, all parameters required for the reconstruction of the final MSPDD results (i.e., the duration of fictitious excitation, sampling frequency and time of the reconstructed signal) are user-defined and are not restricted by the hammer strike and testing device in practice. This means the MSPDD results obtained by various testing equipment can be utilized to build the sample set, which enables the data-driven identification of pile defects. Therefore, the time-series MSPDD results that are derived from original signals processed by TWD theory are utilized to conduct the pile damage detection, including multiple tasks: (1) number of defects below the sensors (**Task 1**); (2) type of defect (i.e., necking or expansion) closest to the sensors (**Task 2**); and (3) degree of the closest defect (**Task 3**). Once these tasks are resolved, the results can provide a detailed description of the actual pile quality and aid in classifying the pile quality.

3.1. Proposed Hybrid Convolutional and Recurrent Neural Network Framework

To conduct the multi-task pile damage detection, a hybrid one-dimensional (1D) convolutional and recurrent neural network is proposed herein to process the time-series MSPDD results. Figure 3 demonstrates the architecture of the proposed multi-task learning framework, which involves two major steps:

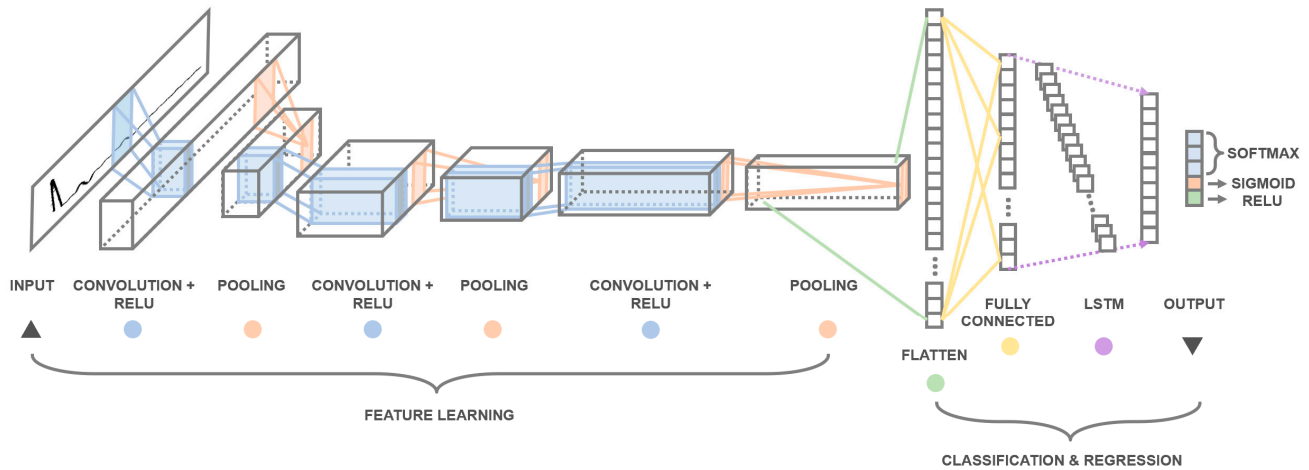


Figure 3. Architecture of hybrid 1D CNN and LSTM framework.

(1) One-dimensional convolutional neural network (CNN)

The time-series MSPDD results (whose length is equal to the user-defined number of sampling points) are input into the 1D convolutional neural network through the input layer. The 1DCNN is employed to automatically extract the features of the time-series signals. The proposed 1DCNN framework incorporates three pairs of convolution and pooling layers. The first convolution layer has 64 convolution kernels of size 5 with strides 1 and valid padding, while the second and third convolution layers have 128 and 256 convolution kernels, respectively, with the same size, strides and padding. The mathematical description of the convolution layer can be summarized as follows [40]:

$$z_i^l = \sigma\left(\sum_j z_j^{l-1} \times w_{ij}^l + b_i^l\right) \quad (6)$$

where z_i^l is the i th feature at layer l ; z_j^{l-1} is the j th feature at layer $(l - 1)$; w_{ij}^l denotes the kernel connecting the j th feature at layer $(l - 1)$ and the i th feature at layer l ; b_i^l is the bias of the i th feature at layer l ; and $\sigma(\cdot)$ denotes the activation function.

The outputs of the convolution layers are activated by Rectified Linear Unit (ReLU) and are then passed as input into their subsequent 1D max-pooling layers with a size of 4. The operation of the 1D max-pooling layer can be expressed as follows [40]:

$$z_p^l = \max_{\forall i \in \Omega} z_i^{l-1} \quad (7)$$

where Ω denotes the pooling region.

(2) Long short-term memory (LSTM) network

The extracted features learned by 1DCNN are first flattened and reshaped, and then passed into the long short-term memory (LSTM) layers. The LSTM network belongs to the category of recurrent neural networks (RNNs) and can be utilized to learn the long-term dependencies of sequential inputs. The long-term memory of the network is achieved

through the cooperation of three gate modules, i.e., forget gate (FG), update gate (UG) and output gate (OG). The operation of each gate module can be expressed as follows [41,42]:

$$\text{FG} : f_t = \sigma(W_f h_{t-1} + U_f x_t) \quad (8)$$

$$\text{UG} : \begin{cases} i_t = \sigma(W_i h_{t-1} + U_i x_t) \\ \tilde{C}_t = \tanh(W_c h_{t-1} + U_c x_t) \end{cases} \quad (9)$$

$$\text{OG} : \begin{cases} C_t = f_t C_{t-1} + i_t \tilde{C}_t \\ o_t = \sigma(W_o h_{t-1} + U_o x_t) \\ h_t = \tanh(C_t) o_t \end{cases} \quad (10)$$

where W_f and U_f are parameter matrices in the forget gate; W_i , W_c and U_i , U_c are parameter matrices in the update gate; W_o and U_o are parameter matrices in the output gate; and x_t , h_t and C_t are the input, hidden state and cell state of the LSTM network at time step t , respectively.

3.2. Multi-Task Learning and Loss Function

The output (i.e., hidden state at the last time step) of the LSTM network is eventually utilized to resolve multiple tasks of pile damage detection as described above. Firstly, the Softmax activation is employed to classify pile damage conditions below the sensors into three categories: intact pile (**Class I**), pile with one defect (**Class II**) and pile with multiple (more than one) defects (**Class III**). The Softmax function can be expressed as follows:

$$\text{Softmax}(z_i) = p_i = \frac{\exp(z_i)}{\sum \exp(z_i)} \quad (11)$$

where the index i of the maximum probability p_i corresponds to the classification of the pile damage conditions.

Secondly, the Sigmoid function is used to conduct the binary defect-type classification (necking or expansion) of the defect closest to sensors, i.e.,

$$\text{Sigmoid}(z_i) = \frac{1}{1 + \exp(-z_i)} \quad (12)$$

Thirdly, the regression prediction of the degree of closest defect is obtained by ReLU activation, whose function is given as

$$\text{ReLU}(z_i) = \max(0, z_i) \quad (13)$$

So far, the output layer of size 5 neurons has been integrated to describe the actual pile quality below the sensors. Table 1 provides some examples of descriptions of output labels. Moreover, if the exact number or specific conditions of multiple defects need to be determined in some cases, it can also be achieved by continuing to lower the sensor position and repeating the MSPDD test. Multiple defects can then be detected one by one from top to bottom. However, in most cases, an RC pile with multiple defects will be directly evaluated as the worst class according to the Chinese Technical Code for Testing of Building Foundations Piles [43].

Table 1. Some examples of descriptions of output labels.

Labels of Outputs	Description (Below Sensors)
[1 0 0 0 0]	There is no defect.
[0 1 0 0 0.31]	There is one defect, whose acoustic impedance value is 31% lower than that of the intact segment.
[0 0 1 1 0.16]	There are multiple defects, and the acoustic impedance value of the closest defect is 16% higher than that of the intact segment.

It is also noted that there exists a priority relationship between multiple tasks. Rationally, the binary classification (**Task 2**) and degree regression (**Task 3**) of the closest pile defect are only discussed when the pile is detected as defective; otherwise, the predictions of the latter two tasks are meaningless. Therefore, to clarify the sequence of multiple tasks and improve the accuracy of classification and regression as described in preceding sections, a loss function J is proposed to facilitate multi-task learning, i.e.,

$$\begin{cases} J_1 = -\sum_{i=1}^3 y_i \cdot \log(p_i) \\ J_2 = -[y_4 \cdot \log(p_4) + (1 - y_4) \cdot \log(1 - p_4)] \\ J_3 = (y_5 - p_5)^2 \\ J = y_1 \cdot J_1 + (y_2 + y_3) \cdot (J_1 + J_2 + J_3) \end{cases} \quad (14)$$

where y_i and p_i denote the i th element of the labeled and predicted output, respectively.

4. Sample Generation Based on Analytical Models

Wu et al. [35] demonstrated the excellent agreement of the reconstructed signals derived from the analytical solution and experimental results. Therefore, it is safe to say the MSPDD results are not sensitive to their sources (e.g., analytical solution, finite element analysis simulation or model test results). Given that the MSPDD results derived from actual integration test projects are insufficient at this point, the multi-channel signals collected by equally spaced sensors are simulated by an analytical solution herein to generate a sufficient number of samples and thus investigate the feasibility of employing the proposed hybrid neural network to conduct the multi-task learning.

The analytical solution to a pile with multiple defects embedded in layered soil when subjected to vertical excitation can be resolved by the scheme of acoustic impedance transfer mechanism (AITM) [11], where the acoustic impedance function Z_i at the top of pile segment i ($i \geq 2$) can be expressed as a function of Z_{i-1} , i.e.,

$$Z_i = \rho_i C_i \lambda_i \cdot \frac{\rho_i C_i \lambda_i \sin(\lambda_i / C_i \cdot l_i) - Z_{i-1} \cos(\lambda_i / C_i \cdot l_i)}{\rho_i C_i \lambda_i \cos(\lambda_i / C_i \cdot l_i) + Z_{i-1} \sin(\lambda_i / C_i \cdot l_i)} \quad (15)$$

where ρ_i , C_i and l_i denote the mass density, one-dimensional elastic wave velocity and length of the pile segment i , respectively; λ_i is a frequency-domain coefficient related to the resistance of soil around pile segment i and can be determined by existing dynamic soil models (e.g., Kelvin–Voigt model [4], Plane-strain model [44], Continuous media considering three-dimensional effects [11,12]).

Once the boundary conditions at the pile top and pile toe are determined, the dynamic responses along the pile shaft at various depths can be thoroughly solved. To obtain a better distribution of a sample set and facilitate multi-task learning, the analytical solution-based sample generation is artificially controlled. Figure 4 displays a flowchart of the generation procedure of various cases for analytical analysis, where α_I and α_{II} denote the occurrence probabilities of various pile conditions; α_1 and α_2 are the occurrence probabilities of the type of the first and second defects below the sensors, respectively; and α_s and α_m are the occurrence probabilities of various soil conditions and type of the intermediate layer, respectively.

The analytical results subject to the generated random cases are added with additive white Gaussian noise (AWGN) to increase the randomness of the raw data. The noise-introduced analytical results are then utilized to simulate the time-series signals collected by multiple equally spaced sensors of the MSPDD test. After the post-processing procedure described in Section 2.2, the simulated multi-channel signals are finally processed into a sample set of the MSPDD results. Figure 5 displays several MSPDD results derived from multi-channel signals simulated by analytical solutions subjected to specific cases, where the reconstructed signals can eliminate the effect of superstructures and thus highlight the

reflections below the sensors. It is also noted that the MSPDD results have already been normalized by introducing the generalized incident wave as clarified in Section 2.2.

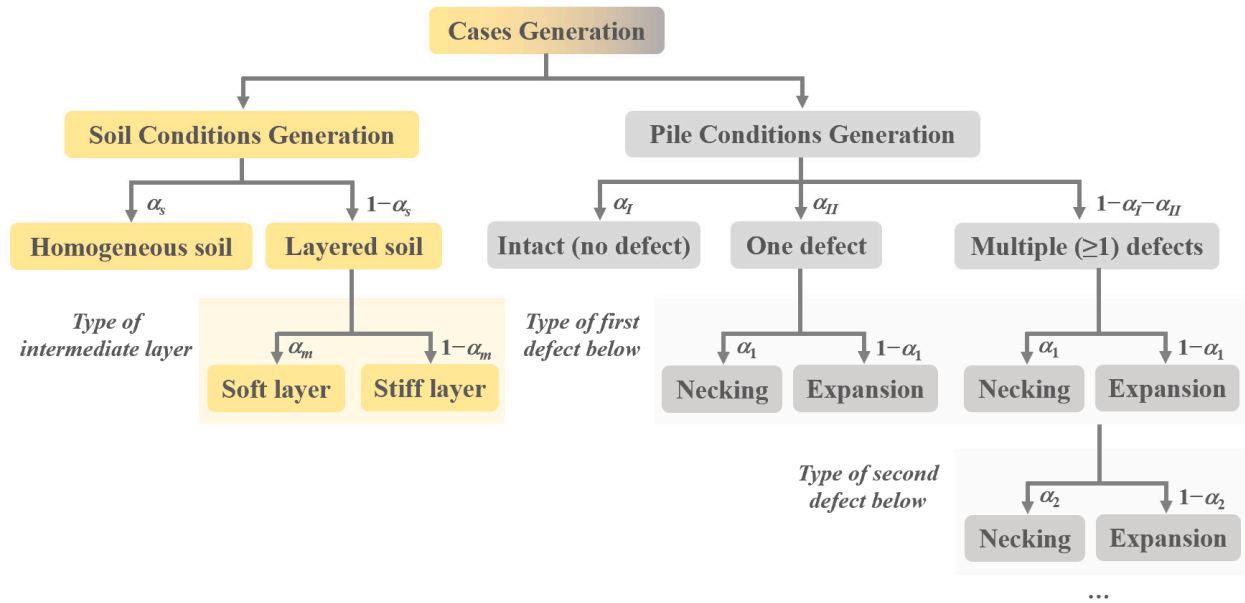


Figure 4. Flowchart of case generation.

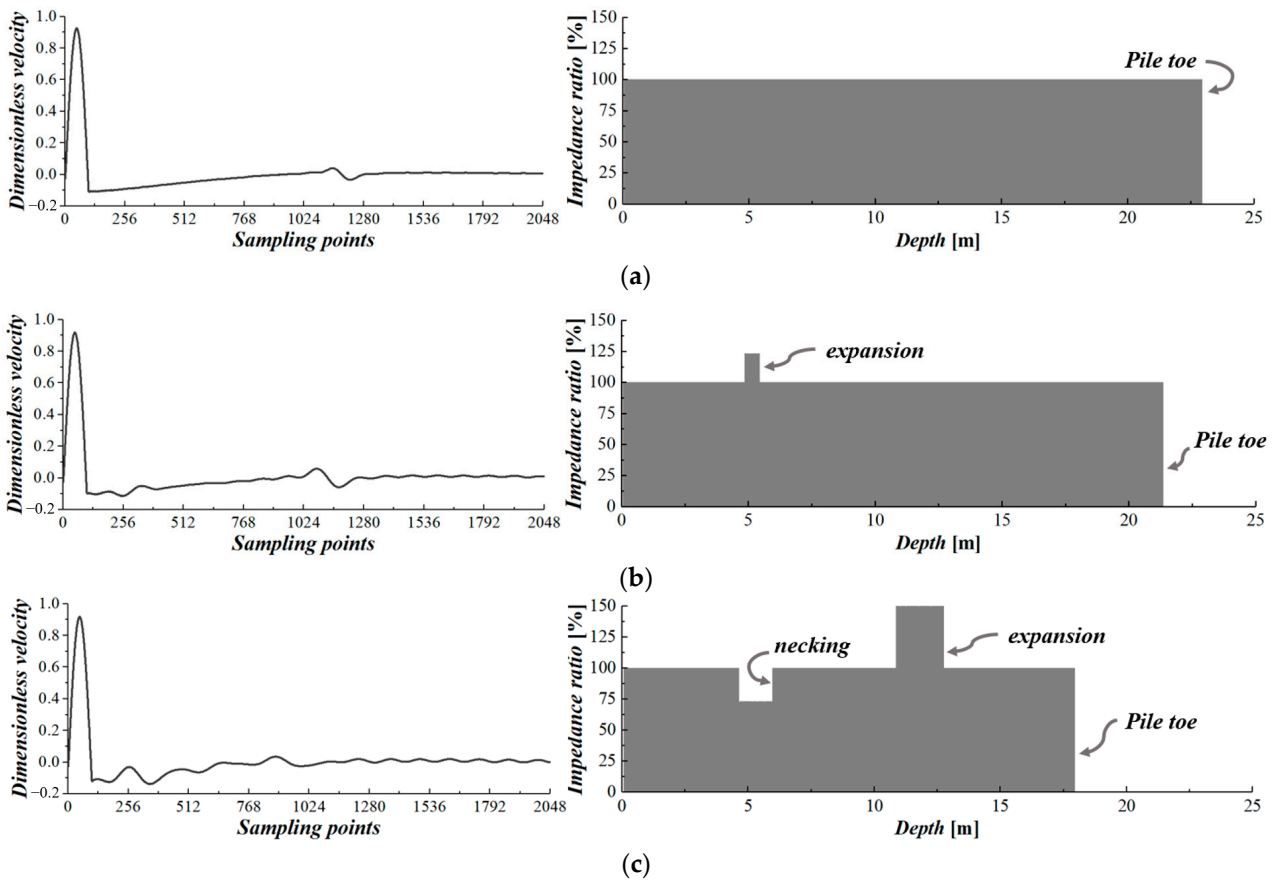


Figure 5. MSPDD results derived from multi-channel signals simulated by analytical solutions: (a) intact pile; (b) pile with one defect; (c) pile with multiple (more than one) defects.

5. Results and Discussion

An analytical solution-based sample set is utilized herein to verify the feasibility of employing the proposed hybrid convolutional and recurrent neural network to conduct multi-task pile damage detection. The sample set is randomly split into training, validation and testing sets (60/20/20%); the parameters of the hybrid neural network are tuned by the training and validation sets, and the performance of the multi-task pile damage detection is evaluated by the testing set. Moreover, the early stopping technique is employed to reduce overfitting without compromising on model accuracy.

Given that the collection of MSPDD results derived from actual projects is time-consuming and labor-intensive, it is reasonable to take the size of the sample set into consideration. Figure 6a–d demonstrate the iterative learning procedure of the loss function considering sample numbers equal to 1000, 2000, 4000 and 8000. As expected, as the number of samples increases, the loss function drops faster and the validation loss derived from the validation set converges to a smaller value, which corresponds to better learning efficiency. Taking advantage of the early stopping technique, the iteration stops when the validation loss has a tendency to increase in later iterations, which can effectively suppress overfitting and strengthen the generalization ability of the model, especially for a small sample set (e.g., Figure 6a).

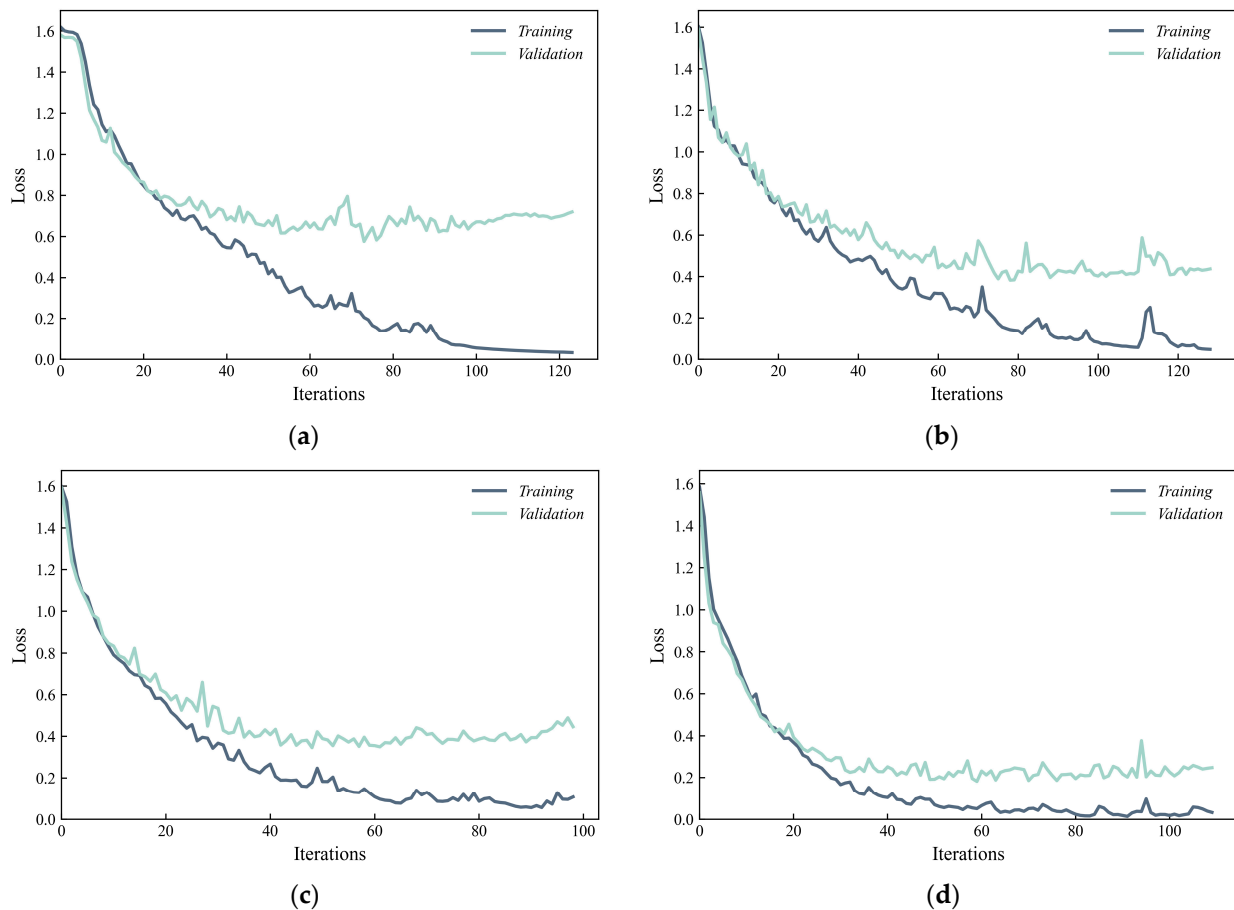


Figure 6. Iterative learning procedure of loss function considering number of samples: (a) 1000; (b) 2000; (c) 4000; (d) 8000 (loss function is expressed in Equation (14)).

Figure 7 displays the overall evaluation of the proposed hybrid neural network in multi-task pile damage detection. Four accuracy metrics are introduced to evaluate the hybrid model performance on specific pile damage detection tasks: (1) Categorical Accuracy (CA) for multi-classification of pile conditions (**Task 1**); (2) Binary Accuracy (BA) for type classification of the closest pile damage (**Task 2**); (3) Mean Squared Error (MSE) accuracy for

degree regression of the closest pile damage (**Task 3**); (4) F1 Score for binary classification (pile is defective or not), i.e., recognition of **Class I**, which is a sub-task of **Task 1** (denoted as **Task 1-I**). The formula for the F1 Score can be expressed as follows:

$$F_1 = 2 \cdot \frac{\text{precision} \cdot \text{recall}}{\text{precision} + \text{recall}} \quad (16)$$

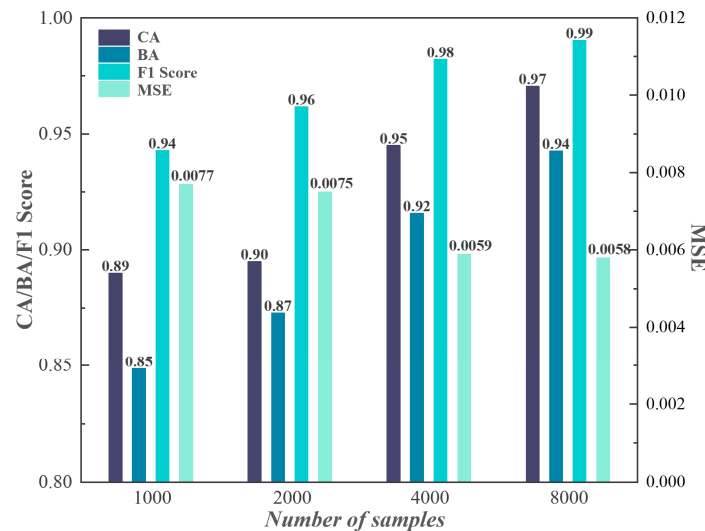


Figure 7. Performance of hybrid neural network on multi-task pile damage detection.

Consistent with the tendency of the loss function, CA, BA and F1 Score values increase and the MSE value decreases as the sample size increases. Fortunately, benefiting from the proposed multi-sensor detection method as well as the multi-task learning framework, the accuracy metrics for small samples (e.g., 1000 in this case) are also satisfactory. Comparing CA, BA and F1 Score values, it is worth noting that the recognition accuracy of **Class I** is better than the Categorical Accuracy of multi-class (**Class I, II and III**), and both are better than the defect-type classification accuracy. This is due to the sequential relation between multiple tasks, where **Task 2** is conducted based on the sub-task of **Task 1** (i.e., **Task 1-I**), while **Task 3** is conducted on the basis of **Task 2**. Although errors from the previous task are passed on to its subsequent task, this scheme also follows the priority of the detection order in an actual project. For the purpose of only identifying whether there are defects below the sensors (i.e., **Task 1-I**), even a small sample set (e.g., 1000 in this case) can obtain an excellent recognition accuracy (F1 Score = 0.94) based on the hybrid model. Furthermore, if the number and type of defects need to be determined in some cases, a larger sample size is required (≥ 4000 in this case) to obtain satisfactory CA (≥ 0.95) and BA (≥ 0.92) values.

Figure 8 further investigates the performance of the proposed model on **Task 1**. As indicated by the F1 Score in Figures 7 and 8a–d, the recognition precision and recall of the intact pile condition (i.e., **Class I**) are satisfactory regardless of the sample size. Only a small proportion of piles with one defect (**Class II**) are misidentified as intact piles (**Class I**), and the proportion continues to decrease to 1.3% as the sample size increases to 8000. In engineering practice, it is quite important to accurately distinguish between intact piles and defective piles (with one or multiple defects), thus the importance of **Task 1-I** even exceeds **Task 1** itself. From this perspective, the hybrid model is competent for the basic task of pile damage detection, and it also performs well in small sample cases. As a comparison, the confusion between the recognition of piles with only one defect (**Class II**) and piles with multiple defects (**Class III**) is more pronounced in this case. However, as the number of samples increases, this confusion also diminishes to a satisfactory level, where the precision/recall rates of **Class II** and **Class III** both exceed 95% when the sample size reaches 8000.

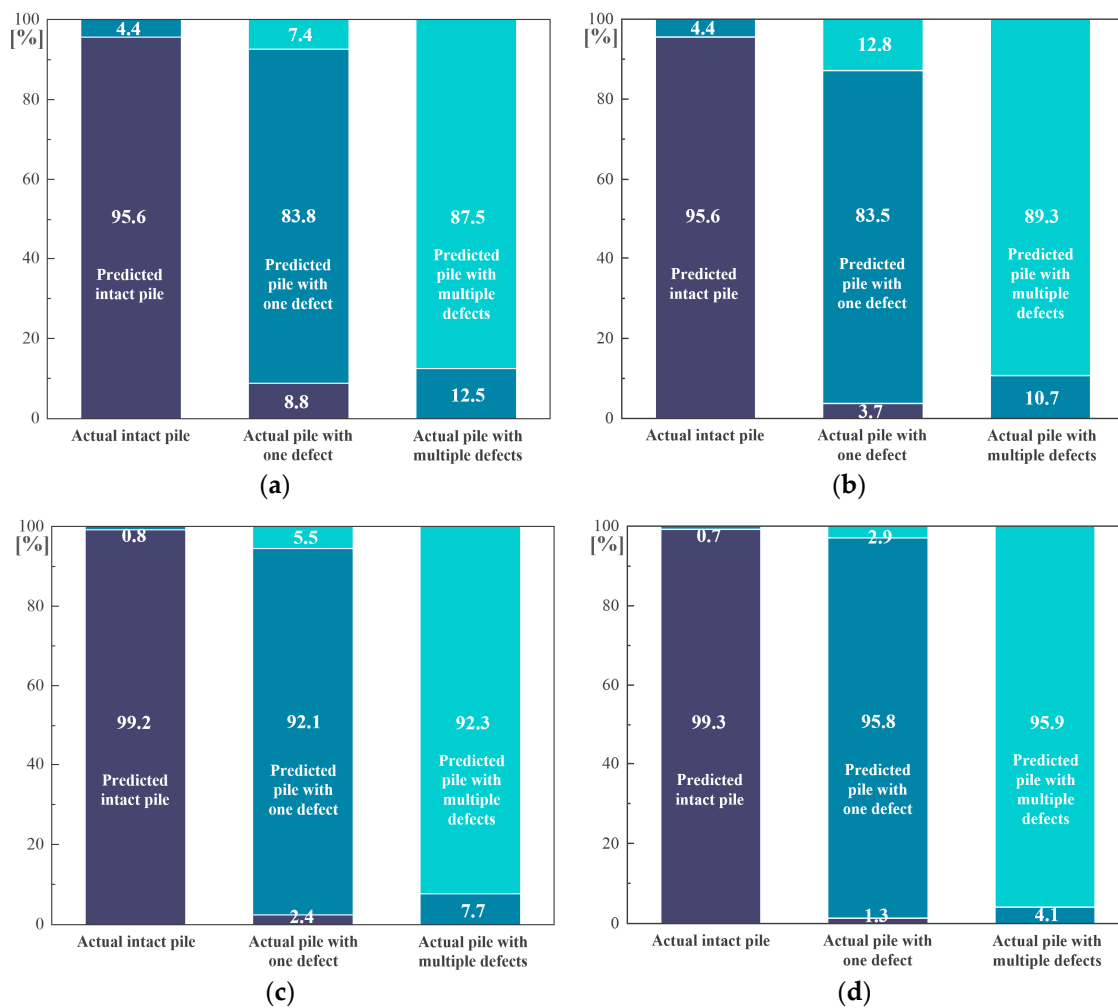


Figure 8. Performance of hybrid neural network in **Task 1** considering numbers of samples equal to (a) 1000; (b) 2000; (c) 4000; (d) 8000.

The performance of the hybrid neural network in **Task 2** is demonstrated in Figure 9a–d. Similarly, the recognition accuracy of defect type increases as the sample size becomes larger. If we take the overall recognition accuracy over 95% as the standard, it is appropriate to construct a sample set of more than 4000 samples to conduct this task. It is also noted that the type recognition of the defect of **Class III** performs better than that of **Class II**, while the accuracy of expansion recognition is also higher than that of necking recognition. The reason for this phenomenon may be that the reflection caused by a necking defect is confused with the pile toe reflection for friction piles, especially when there is only one defect between the sensors and the pile toe.

Figure 10 displays the performance of the hybrid neural network in **Task 3**, where the percentage deviation of the predicted defect degree is demonstrated by the box plot. The deviations corresponding to the medians derived from different sample sizes are basically lower than 20%. As the sample size increases, the mean/median values decrease while the box/whisker range almost remains the same, which means a larger sample size is not beneficial for reducing the variance. This is because the regression of the defect degree is inevitably affected by previous tasks (i.e., residual term of the loss function), and the predicted value output from the hybrid neural network can only be used as a reference value; however, this is sufficient for the detailed description of the pile quality since the number and type of defects have been determined.

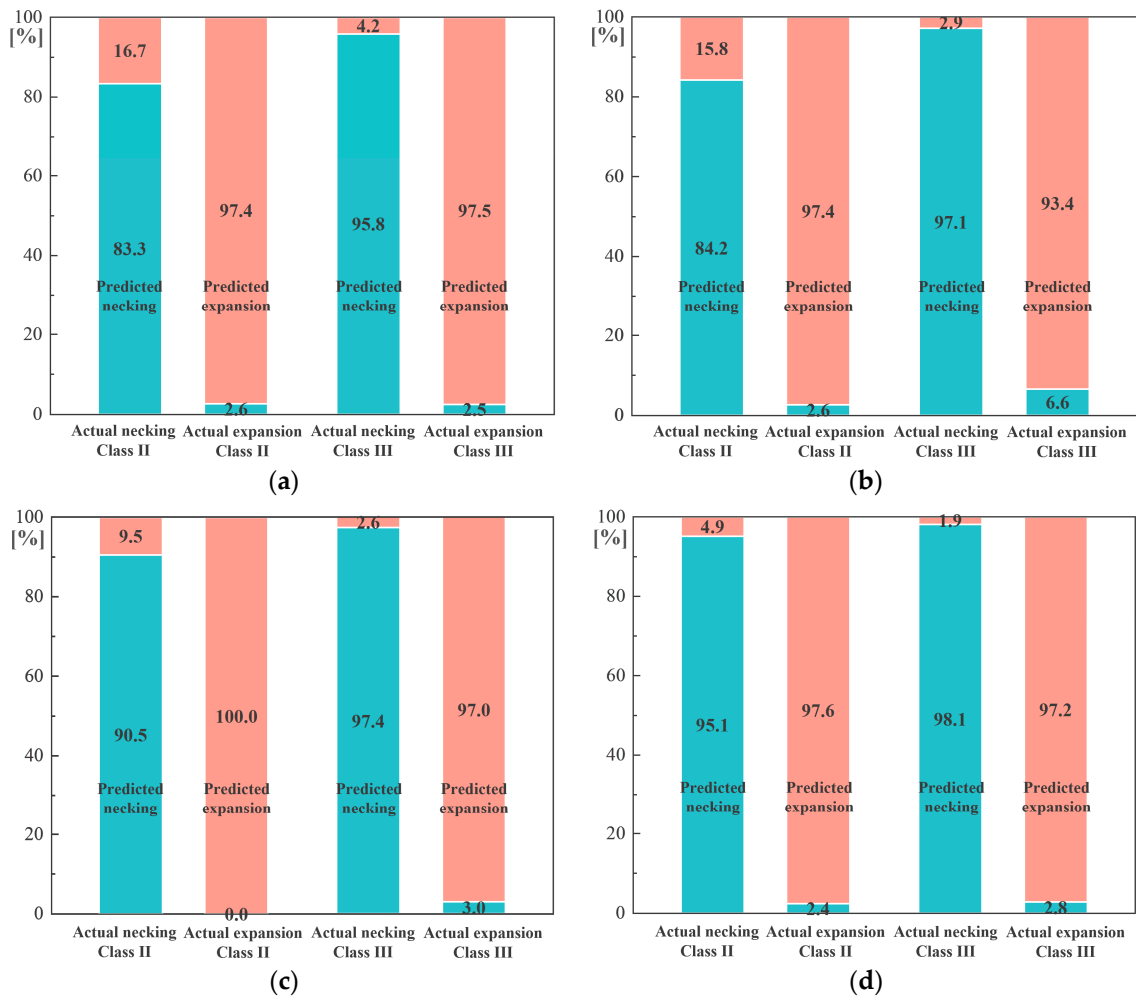


Figure 9. Performance of hybrid neural network in Task 2 considering numbers of samples equal to (a) 1000; (b) 2000; (c) 4000; (d) 8000.

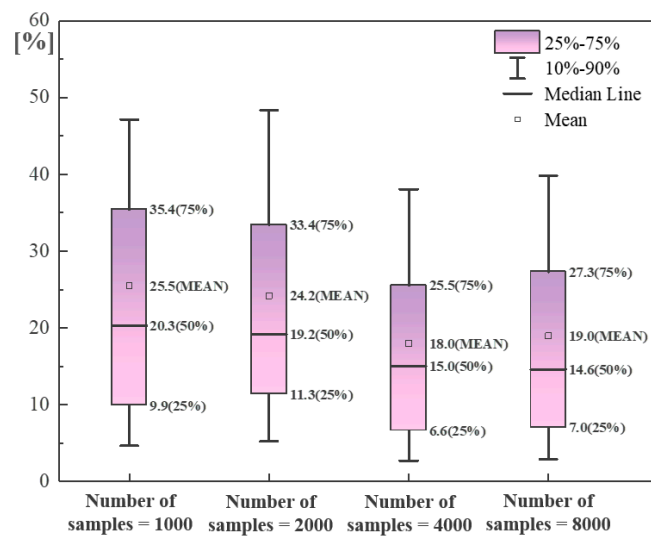


Figure 10. Performance of hybrid neural network in Task 3.

6. Conclusions

- (1) A novel multi-sensor pile damage detection (MSPDD) method is proposed in this paper to evaluate the integrity of onshore and offshore pile foundations, while the trav-

eling wave decomposition (TWD) theory is utilized to implement the post-processing for a series of signals collected by multiple sensors. The reconstructed MSPDD results are then utilized to conduct automatic pile damage detection with multiple tasks.

- (2) A hybrid one-dimensional (1D) convolutional and recurrent neural network is developed for the time-series MSPDD results, and a loss function is proposed to clarify the sequence between multiple tasks and therefore facilitate multi-task learning. Then, an analytical solution-based sample set is utilized to verify the feasibility of employing the hybrid model to conduct multi-task pile damage detection.
- (3) Benefiting from the proposed multi-sensor detection method as well as the multi-task learning framework, the accuracy metrics derived from different sample sizes are satisfactory. For the purpose of only identifying whether there are defects below the sensors (i.e., **Task 1-I**), even a small sample set (e.g., 1000 in this case) can obtain an excellent recognition accuracy (F1 Score = 0.94) based on the hybrid model. If the number and type of defects need to be determined in some cases, a larger sample size is required (e.g., ≥ 4000 in this case) to obtain satisfactory CA (≥ 0.95) and BA (≥ 0.92) values.
- (4) The recognition accuracy of defect type increases as the sample size becomes larger. It is appropriate to construct a sample set of more than 4000 samples to reach 95% overall recognition accuracy, where the accuracy of expansion recognition is higher than that of necking recognition. The deviations of predicted defect degrees corresponding to the medians are basically lower than 20%, which can provide a more detailed description of the pile quality together with the number and type of defects.

Author Contributions: Writing—Original draft, J.W.; Writing—Review and editing, M.H.E.N. and K.W. All authors have read and agreed to the published version of the manuscript.

Funding: This research was funded by the Natural Science Foundation of Zhejiang Province (grant no. LTGG24E080001) and the National Natural Science Foundation of China (grant Nos. 52108349 and 52178358).

Institutional Review Board Statement: Not applicable.

Informed Consent Statement: Not applicable.

Data Availability Statement: Data are contained within the article.

Conflicts of Interest: The authors declare no conflict of interest.

References

1. Massoudi, N.; Teferra, W. Non-destructive testing of piles using the low strain integrity method. In Proceedings of the 15th International Conference on Case Histories in Geotechnical Engineering, New York, NY, USA, 13–17 April 2004.
2. Ding, X.; Liu, H.; Liu, J.; Chen, Y. Wave propagation in a pipe pile for low-strain integrity testing. *J. Eng. Mech.* **2011**, *137*, 598–609. [[CrossRef](#)]
3. Zheng, C.; Liu, H.; Ding, X.; Kouretzis, G.P.; Sloan, S.W.; Poulos, H.G. Non-axisymmetric response of piles in low-strain integrity testing. *Géotechnique* **2017**, *67*, 181–186. [[CrossRef](#)]
4. Wu, J.T.; Wang, K.H.; Gao, L.; Xiao, S. Study on longitudinal vibration of a pile with variable sectional acoustic impedance by integral transformation. *Acta Geotech.* **2019**, *14*, 1857–1870. [[CrossRef](#)]
5. Chernauskas, L.R.; Paikowsky, S.G. Defect detection and examination of large drilled shafts using a new cross-hole sonic logging system. In *Performance Confirmation of Constructed Geotechnical Facilities*; American Society of Civil Engineers: Reston, VA, USA, 2000; pp. 66–83.
6. Li, D.Q.; Zhang, L.M.; Tang, W.H. Reliability evaluation of cross-hole sonic logging for bored pile integrity. *J. Geotech. Geoenvironmental Eng.* **2005**, *131*, 1130–1138. [[CrossRef](#)]
7. White, B.; Nagy, M.; Allin, R. Comparing cross-hole sonic logging and low-strain integrity testing results. In Proceedings of the Eighth International Conference on the Application of Stress Wave Theory to Piles, Lisbon, Portugal, 8–10 September 2008; pp. 471–476.
8. Abishdid, C.; Hajali, M. Detecting location of construction defects in drilled shafts using frequency tomography analysis of cross-hole sonic logging. In *Computing in Civil and Building Engineering*; American Society of Civil Engineers: Reston, VA, USA, 2014; pp. 1723–1730.
9. Davis, A.G. Nondestructive evaluation of existing deep foundations. *J. Perform. Constr. Facil.* **1995**, *9*, 57–74. [[CrossRef](#)]

10. Sack, D.A.; Slaughter, S.H.; Olson, L.D. Combined measurement of unknown foundation depths and soil properties with nondestructive evaluation methods. *Transp. Res. Rec.* **2004**, *1868*, 76–80. [[CrossRef](#)]
11. Wu, J.; Wang, K.; El Naggar, M.H. Dynamic soil reactions around pile-fictitious soil pile coupled model and its application in parallel seismic method. *Comput. Geotech.* **2019**, *110*, 44–56. [[CrossRef](#)]
12. Wu, J.; El Naggar, M.H.; Wang, K. Analytical model for laterally loaded soil-extended pile shaft applied to verifying the applicability of lateral PS method. *J. Geotech. Geoenvironmental Eng.* **2021**, *147*, 04021103. [[CrossRef](#)]
13. Yang, J.; Sun, X.L.; Bian, D.C.; Shao, J.X. Large-scale model test for detecting pile defects using the parallel seismic method. *Soil Dyn. Earthq. Eng.* **2020**, *139*, 106300. [[CrossRef](#)]
14. Shmurak, D.V.; Churkin, A.A.; Lozovsky, I.N.; Zhostkov, R.A. Spectral Analysis of Parallel Seismic Method Data for Surveying Underground Structures. *Bull. Russ. Acad. Sci. Phys.* **2022**, *86*, 79–82. [[CrossRef](#)]
15. Wu, J.; El Naggar, M.H.; Wang, K.; Wu, W. Lateral vibration characteristics of an extended pile shaft under low-strain integrity test. *Soil Dyn. Earthq. Eng.* **2019**, *126*, 105812. [[CrossRef](#)]
16. Wu, J.; El Naggar, M.H.; Wang, K.; Liu, X. Analytical Study of Employing Low-Strain Lateral Pile Integrity Test on a Defective Extended Pile Shaft. *J. Eng. Mech.* **2020**, *146*, 04020103. [[CrossRef](#)]
17. Farrar, C.R.; Worden, K. An introduction to structural health monitoring. *Philos. Trans. R. Soc. A Math. Phys. Eng. Sci.* **2007**, *365*, 303–315. [[CrossRef](#)] [[PubMed](#)]
18. Worden, K.; Manson, G. The application of machine learning to structural health monitoring. *Philos. Trans. R. Soc. A Math. Phys. Eng. Sci.* **2007**, *365*, 515–537. [[CrossRef](#)] [[PubMed](#)]
19. Finotti, R.P.; Cury, A.A.; Barbosa, F.D.S. An SHM approach using machine learning and statistical indicators extracted from raw dynamic measurements. *Lat. Am. J. Solids Struct.* **2019**, *16*, e165. [[CrossRef](#)]
20. Tran-Ngoc, H.; Khatir, S.; Ho-Khac, H.; De Roeck, G.; Bui-Tien, T.; Wahab, M.A. Efficient Artificial neural networks based on a hybrid metaheuristic optimization algorithm for damage detection in laminated composite structures. *Compos. Struct.* **2021**, *262*, 113339. [[CrossRef](#)]
21. Kingma, D.P.; Salimans, T.; Welling, M. Variational dropout and the local reparameterization trick. In *Advances in Neural Information Processing Systems 28*; MIT Press: Cambridge, MA, USA, 2015.
22. Nguyen, T.H.; Vu, A.T. Evaluating structural safety of trusses using Machine Learning. *Frat. Integrità Strutt.* **2021**, *15*, 308–318. [[CrossRef](#)]
23. González, M.P.; Zapico, J.L. Seismic damage identification in buildings using neural networks and modal data. *Comput. Struct.* **2008**, *86*, 416–426. [[CrossRef](#)]
24. Naresh, M.; Kumar, V.; Pal, J. A machine learning approach for health monitoring of a steel frame structure using statistical features of vibration data. *Asian J. Civ. Eng.* **2023**, *25*, 39–49. [[CrossRef](#)]
25. Chun, P.J.; Yamashita, H.; Furukawa, S. Bridge damage severity quantification using multipoint acceleration measurement and artificial neural networks. *Shock. Vib.* **2015**, *2015*, 789384. [[CrossRef](#)]
26. Malekjafarian, A.; Golpayegani, F.; Moloney, C.; Clarke, S. A machine learning approach to bridge-damage detection using responses measured on a passing vehicle. *Sensors* **2019**, *19*, 4035. [[CrossRef](#)]
27. Parisi, F.; Mangini, A.M.; Fanti, M.P.; Adam, J.M. Automated location of steel truss bridge damage using machine learning and raw strain sensor data. *Autom. Constr.* **2022**, *138*, 104249. [[CrossRef](#)]
28. HosseinAbadi, H.Z.; Amirfattahi, R.; Nazari, B.; Mirdamadi, H.R.; Atashipour, S.A. GUV-based structural damage detection using WPT statistical features and multiclass SVM. *Appl. Acoust.* **2014**, *86*, 59–70. [[CrossRef](#)]
29. Khatir, S.; Boutchicha, D.; Le Thanh, C.; Tran-Ngoc, H.; Nguyen, T.N.; Abdel-Wahab, M. Improved ANN technique combined with Jaya algorithm for crack identification in plates using XIGA and experimental analysis. *Theor. Appl. Fract. Mech.* **2020**, *107*, 102554. [[CrossRef](#)]
30. Khatir, S.; Khatir, T.; Boutchicha, D.; Le Thanh, C.; Tran, N.H.; Bui, T.Q.; Abdel Wahab, M. An efficient hybrid TLBO-PSO-ANN for fast damage identification in steel beam structures using IGA. *Smart Struct. Syst.* **2020**, *25*, 605–617.
31. Bui-Tien, T.; Bui-Ngoc, D.; Nguyen-Tran, H.; Nguyen-Ngoc, L.; Tran-Ngoc, H.; Tran-Viet, H. Damage detection in structural health monitoring using hybrid convolution neural network and recurrent neural network. *Frat. Integrità Strutt.* **2022**, *16*, 461–470. [[CrossRef](#)]
32. Teng, S.; Chen, G.; Liu, Z.; Cheng, L.; Sun, X. Multi-sensor and decision-level fusion-based structural damage detection using a one-dimensional convolutional neural network. *Sensors* **2021**, *21*, 3950. [[CrossRef](#)] [[PubMed](#)]
33. Yu, H.; Seno, A.H.; Sharif Khodaei, Z.; Aliabadi, M.F. Structural Health Monitoring Impact Classification Method Based on Bayesian Neural Network. *Polymers* **2022**, *14*, 3947. [[CrossRef](#)] [[PubMed](#)]
34. Jiang, C.; Zhou, Q.; Lei, J.; Wang, X. A Two-Stage Structural Damage Detection Method Based on 1D-CNN and SVM. *Appl. Sci.* **2022**, *12*, 10394. [[CrossRef](#)]
35. Wu, J.; El Naggar, M.H.; Ge, J.; Wang, K.; Zhao, S. Multipoint Traveling Wave Decomposition Method and Its Application in Extended Pile Shaft Integrity Test. *J. Geotech. Geoenvironmental Eng.* **2021**, *147*, 04021128. [[CrossRef](#)]
36. Wu, J.; El Naggar, M.H.; Wang, K. Pile Damage Detection Using Machine Learning with the Multipoint Traveling Wave Decomposition Method. *Sensors* **2023**, *23*, 8308. [[CrossRef](#)]

37. Gaudio, D.; Juntae, S.; Stuart, H.; Giulia, V.; Gopal, M. 3D nonlinear dynamic Finite Element analysis of onshore wind turbines on pile foundation resting on liquefiable soils. In Proceedings of the 10th European Conference on Numerical Methods in Geotechnical Engineering, NUMGE 2023, London, UK, 26–28 June 2023; pp. 1–6.
38. Liang, F.; Jia, X.; Zhang, H.; Wang, C.; Shen, P. Seismic responses of offshore wind turbines based on a lumped parameter model subjected to complex marine loads at scoured sites. *Ocean. Eng.* **2024**, *116808*. [[CrossRef](#)]
39. Zheng, H.; Zhang, H.; Liang, F.; Li, L. Numerical investigation on lateral monotonic and cyclic responses of scoured rigid monopile based on an integrated bounding surface model. *Comput. Geotech.* **2024**, *166*, 105997. [[CrossRef](#)]
40. Goodfellow, I.; Bengio, Y.; Courville, A. *Deep Learning*; MIT Press: Cambridge, MA, USA, 2016.
41. Yu, Y.; Si, X.; Hu, C.; Zhang, J. A review of recurrent neural networks: LSTM cells and network architectures. *Neural Comput.* **2019**, *31*, 1235–1270. [[CrossRef](#)] [[PubMed](#)]
42. Sherstinsky, A. Fundamentals of recurrent neural network (RNN) and long short-term memory (LSTM) network. *Phys. D Nonlinear Phenom.* **2020**, *404*, 132306. [[CrossRef](#)]
43. *JGJ 106*; Technical Code for Building Pile Foundation. The Professional Standards Compilation Group of People's Republic of China: Beijing, China, 2014.
44. Novak, M.; Aboul-Ella, F.; Nogami, T. Dynamic soil reactions for plane strain case. *J. Eng. Mech. Div.* **1978**, *104*, 953–959. [[CrossRef](#)]

Disclaimer/Publisher's Note: The statements, opinions and data contained in all publications are solely those of the individual author(s) and contributor(s) and not of MDPI and/or the editor(s). MDPI and/or the editor(s) disclaim responsibility for any injury to people or property resulting from any ideas, methods, instructions or products referred to in the content.